Modeling of [^{18}F]-FHBG in Tumor and Normal Tissues
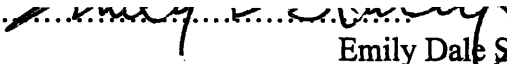
By

Emily Dale Slutsky

SUBMITTED TO THE DEPARTMENT OF NUCLEAR SCIENCE
AND ENGINEERING
IN PARTIAL FULFILLMENT OF THE REQUIREMENTS FOR THE DEGREE OF

BACHELOR OF SICENCE IN NUCLEAR SCIENCE AND ENGINEERING
AT THE
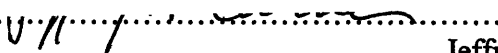MASSACHUSETTS INSTITUTE OF TECHNOLOGY
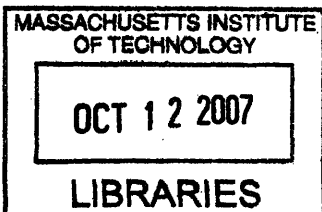
MAY, 2007

[June 2007]

Signature of Author: ....

Emily Dale Slutsky
Department of Nuclear Science and Engineering
May 11, 2007

Certified by: ....

Anna-Liisa Brownell
Associate Professor of Radiology
Massachusetts General Hospital
Thesis Supervisor

Certified by: ....

Jeffrey A. Coderre
Associate Professor of Nuclear Science and Engineering
Thesis Reader

Accepted by: ....

David G. Cory
Professor of Nuclear Science and Engineering
Chairman, NSE Committee for Undergraduate Studies

Modeling of [^{18}F]FHBG in Tumor and Normal Tissues

By

Emily Dale Slutsky

Submitted to the Department of Nuclear Science and Engineering on May 18, 2007
In Partial Fulfillment of the Requirements for the Degree of
Bachelor of Science in Nuclear Science and Engineering

ABSTRACT

The development of new, non-invasive approaches for the treatment of tumors has led to the emergence of oncolytic virus therapy. Viruses have been engineered to preferentially target tumor cells. The efficiency and safety of this cancer treatment is dependent upon selective viral replication within cancer cells. In order for viral oncolysis to be successful in the clinical setting, the biodistribution of viral replication must be quantified. This study has used an enzyme-based positron emission tomography (PET) reporter system to trace the viral replication of herpes simplex virus (HSV)-1. [^{18}F]FHBG was used as the substrate for the HSV-1 enzyme product – thymidine kinase (TK) – in order for PET imaging technique to identity sites of HSV-1 TK activity. The imaged mice were divided into three groups: a control group with no tumor growth and no viral injection, a control group with no tumor growth and viral injection, and an experimental group with both tumor growth and viral injection. The time-activity curves of [^{18}F]FHBG accumulation in the heart, muscle, liver, kidneys, brain, and tumor were plotted for all three groups. A 3-Compartmental Model for the kinetics of [^{18}F]FHBG accumulation within each of the organs was coded using MATLAB, with COMKAT implementation. The time-activity curves were fitted and the kinetic parameters k_1, k_2, and k_3 were calculated. A unified model was additionally presented as a final verification of the calculated parameters. The 3-Comparmental Model developed in this study proved applicable and accurate, with significant applications to interpreting the behavior of specific organs and overall organ systems during viral oncolysis. The qualitative observations formed on the basis of quantitative results have important consequences on the safety and *in vivo* monitoring of oncolytic virus therapy.

Thesis Supervisor: Anna-Liisa Brownell, Ph.D.
Title: Associate Professor of Radiology

Acknowledgements

Contents

List of Figures

List of Tables

1. Introduction

Viral oncolysis represents a unique strategy to exploit the natural process of intracellular viral replication to kill tumor cells. In the early 20th century it was noted that patients with various malignant tumors experienced tumor regression after receiving a rabies vaccination or an affliction with a viral illness [1]. Later, experiments on animals confirmed that viruses are capable of replicating in and lysing tumors [2]. Although oncolytic viruses mediate antitumor activity through a variety of mechanisms, this study will focus on the expression of transgenes (genetic material which has been transferred from one organism to another) inserted into the viral genome. As the virus amplifies through successive cycles of replication and infection of neighboring cells, there is a concomitant amplification of transgene expression [2].

Reporter genes can be used to monitor transgenic reporter gene expression *in vivo*. PET technology utilizes molecular probes labeled with positron-emitting radioisotopes (e.g., fluorine-18 with a half-life of 110 minutes). PET probes typically are either positron-labeled ligands for receptors or positron-labeled substrates for intracellular enzymes. PET reporter gene imaging allows monitoring of the location(s), magnitude, and duration of therapeutic gene expressions, by using vectors for DNA delivery. To non-invasively image biological processes in small animals such as mice, microPET technology with volumetric resolution of approximately 4.1mm^3 has been developed [3].

The reporter gene selected for this study is the gene responsible for the expression of Herpes Simplex Virus thymidine kinase (HSV1-TK), an enzyme that is derived from the Herpes Simplex Virus (HSV-1) and that is deficient in mammalian cells. The Herpes

Simplex Virus is visualized in *Figure 1-1*. HSV1-tk has a large transgene capacity and the virus does not integrate its genome into the cellular genome. HSV1-tk can phosphorylate a range of substrates including DNA precursor analogs such as acycloguanosines (e.g., acyclovir, ganciclovir, penciclovir) and a uracil derivative [e.g., 2'- fluoro-2'-deoxy-1-β-arabinofuranosyl-5-iodouracil (FIAU)].
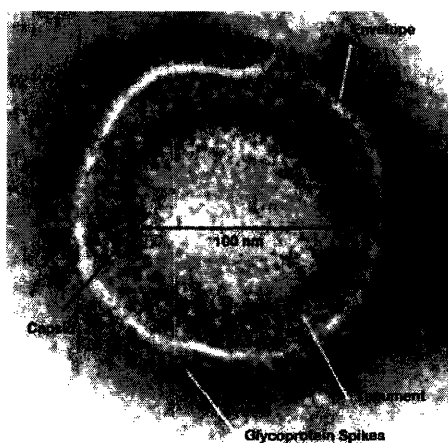
Figure 1-1. **Image of Herpes Simplex Virus-1 with scale [4].**

In relevance to this study, viral thymidine kinase differs from mammalian thymidine kinase by its ability to metabolize guanine derivatives. As a result, 9-[4-[^{18}F]fluoro-3-(hydroxymethyl)butyl]guanine ([^{18}F]FHBG) has been used as a reporter probe to image expression of HSV1-tk reporter gene in living animals in this study.

1.1 *Tumor Destruction by Oncolytic Viruses*

As aforementioned, viruses infect tumor cells through a variety of mechanisms. Viruses may directly destroy cells as a result of viral replication, with progeny virion infecting adjacent cells and destroying them by a similar process. As a second mechanism, some viruses express proteins during their replicative cycle that are cytotoxic

to tumor cells. Finally, viruses, such as the HSV-1 that is explored in this investigation, infect tumor cells through transgenic capability. In addition, viral replication results in an amplification of the original dose, which continues until subject to the organism's immunal response, or lack of susceptible cells.

HSV-1 is an enveloped, double-stranded DNA virus with a genome size of 152 kb. As much as 30 kb of the genome may be replaced by transgenes in replication-defective HSV-1 mutants, allowing for delivery of multiple transgenes. HSV-1 rarely produces illness in immunogically healthy adults. Anti-herpetic agents such as acyclovir are available that provide a safety mechanism to shut off viral replication if cytotoxicity ensues. HSV-1 does not integrate its genome into the cellular genome, as does a retrovirus for example, and therefore insertional mutagenesis is not a concern.

HSV-1 is organized into unique long (U_L) and unique short (U_S) sequences flanked by inverted repeat sequences. TK production is encoded by U_L23. A brief schematic of the virus is included in *Figure 1*-2. The first report of an oncolytic application of HSV-1 described use of a mutant, *dlsptk*, which is defective in TK expression [5]. The mutant, *dlsptk*, attempted to bypass the virus' requirement for U_L23. Mice with tumors treated with *dlsptk* had improved survival compared to control mice, but the virus was neurotoxic at high titers, thereby making the mutant ineffective for clinical use. The findings suggest that maintaining a functional tk gene in HSV-1 mutants is an imperative, built-in safety feature for clinical use.

The transgenic capabilities of HSV-1 create cells that are actively transcribing and translating the TK-generating mRNA. Cancer cells with unreliable control mechanisms exhibit significantly different kinetic profiles when compared to healthy cells.
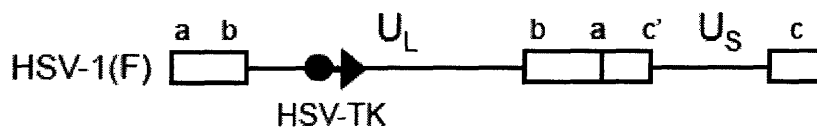
Figure 1-2. **Genomic structure for wild-type HSV-1(F).** The tk promoter region of the strain virus is highlighted [6].

1.2 *Structure and Function of [^{18}F]FHBG*

[^{18}F]FHBG is a radiolabeled analog of penciclovir (PCV), a compound very similar in structure to acyclovir (ACV) and ganiclovir (GCV). PCV is a guanine analogue antiviral drug predominantly used for treatment of various herpesvirus infections, which exhibits low toxicity and good selectivity. ACV has been shown to cross the human erythrocyte membrane by nucleobase transporters and GCV has been shown to cross the human erythrocyte membrane by both nucelobase and nucleoside transporters [7,8]. Therefore, it is likely that [^{18}F]FHBG uses nucleobase or nucleotide transporters to enter and exit the cells. *Figure 1-3* presents the molecular structure of [^{18}F]FHBG.
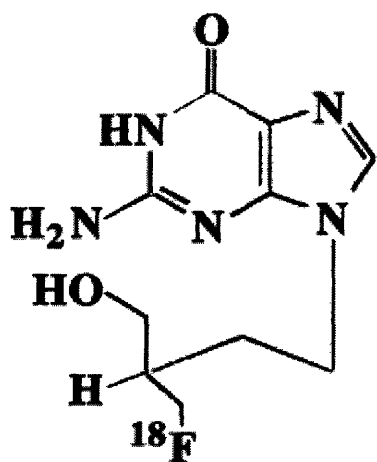
Figure 1-3. **Structure of [^{18}F]FHBG.** Presence of fluorine atom renders molecule chiral

1.3 Biological Mechanism for Imaging

A general paradigm for noninvasive reporter gene imaging using radiolabeled probes was initially described in 1995 [9]. The paradigm requires the appropriate combination of a reporter/marker transgene and probe. The reporter transgene usually encodes for an enzyme (e.g. HSV1-TK) that selectively metabolizes the radiolabeled probe and results in its entrapment and accumulation in the transduced cell. Enzymatic amplification of the signal (e.g., level of radioactivity) facilitates imaging the location and magnitude of reporter gene expression.

HSV1-tk is the reporter gene most commonly used in current molecular imaging studies using radiolabeled probes and PET imaging due to several properties of the virus that render it well suited for viral oncolysis: high transgene capacity, lack of integration into the cellular genome, prevalence in the population, sensitivity to specific antiviral compounds (e.g., acyclovir), and rarity with which it produces severe medical illness. The HSV1-tk gene products are proteins (enzymes) that have less substrate specificity than mammalian TK. The HSV1-TK phosphorylates a wider range of compounds than mammalian TK. This difference between mammalian and viral TK enzymes permits the development and use of radiolabeled probes that will specifically label cells expressing HSV1-TK.

Figure 1-4 depicts the schematic for imaging HSV1-tk reporter gene expression with reporter probe FHBG. The HSV1-tk gene complex is introduced into target cells by a viral vector. Inside the targeted cell, the HSV1-tk gene is transcribed to HSV1-tk mRNA and then translated in the ribosomes to the enzyme, HSV1-TK. After administration of complimentary radiolabeled reporter probe FHBG and transport into the

cell, the probe is phosphorylated by HSV1-TK. The phosphorylated radiolabeled report probe does not readily cross the membrane; it is trapped and accumulates within the cell. Thus, the magnitude of marker/reporter probe accumulation reflects the level of HSV1-TK enzyme activity and the level of HSV1-tk gene expression.
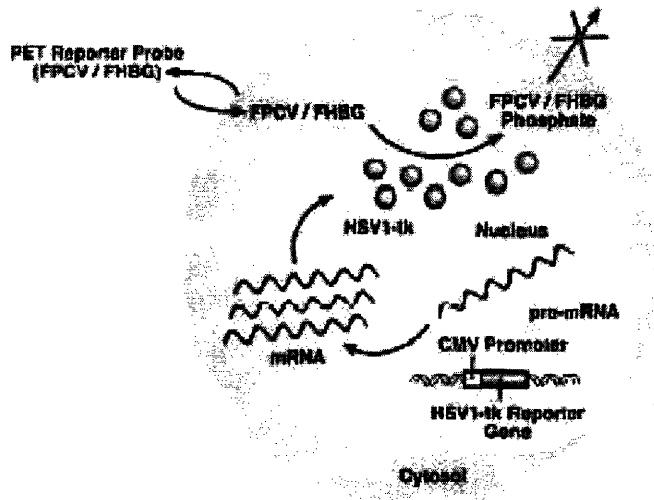
Figure 1-4. Schematic for HSV1-tk imaging [4]

2. Methods and Materials

2.1 Biological Preparation

HSV-TK-transformed MC26 murine colon carcinoma cells were created by subcloning sr39tk cDNA into an expression vector driven by an SV40 promoter. MC26 cells were transfected and stable clones were isolated and screened for thymidine kinase expression using hypoxanthine-aminopterin-thymine medium and by assessing their sensitivity to ganciclovir. Transformants were selected to show a 150-fold greater accumulation of [18F]FHBG compared with nontransformed MC26 cells.

2.2 Animal Studies

To induce the formation of flank tumors in BALB/c mice a suspension of 1×10^5 MC26 cells in 100-μL phosphate-buffered saline (PBS) without Ca^{2+} or Mg^{2+} was inoculated into the right upper flank, subcutaneously. Seven days later, the virus was injected into the tumor. Tens of control and tumor mice were infected with HSV-1 and imaged over a period of three years. The resulting images were collected and analyzed until microPET scan technique was perfected.

The scope of interest of this paper was the data analysis of three mice groups: **Group A** with no virus injected and no tumor growth, **Group B** injected with virus but with no tumor growth, and **Group C** with tumor growth and virus injection. Groups A and B can be said to serve as basic controls. Groups A and B consisted of two mice each, while Group C became a classification for four specimens. Each group was injected with a viral dose of 10^7 plaque-forming units (pfu), approximately 24 hours before screening.

2.3 MicroPET Imaging

Seven days later, once the tumors reached a size of approximately 5 mm, the viral dosage was given by injection directly into the center of the tumor. The mice were anesthetized with isoflurane (1-1.5%) with an oxygen flow rate of 2 L/min (depicted in *Figure 2-1*). The efficacy of the anesthesia was monitored by respiratory rate, as well as motor reflex and eye movement. The radioligand, [18F]FHBG, was administered through the tail vein with a 30 gauge needle, at a volume that ranged from 20 to 60 μL. Heparin sodium at 6 units/mL was additionally injected through the tail to maintain patency of the blood vessels. The author was present and an active participant in many of these injections.
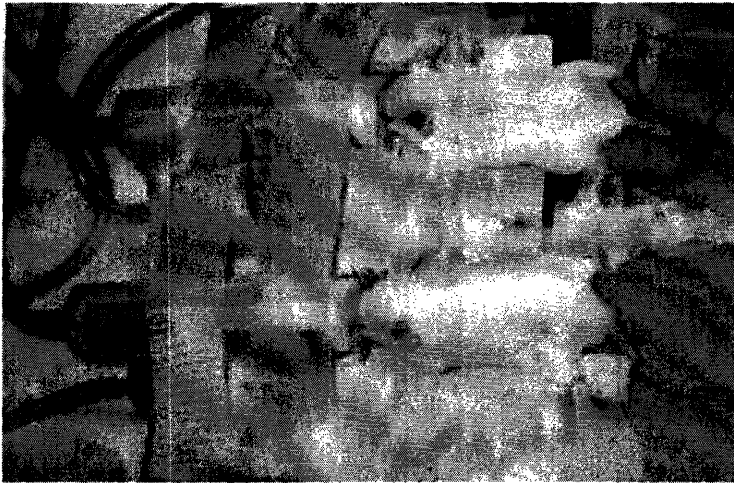
Figure 2-1. **Anesthesia of BALB/c mice with isoflurane [4]**

Animals were positioned into the microPET scanner as pictured in *Figure 2-2*, with the long axis of the body parallel to the long axis of the scanner (microPET-P4, Concorde Microsystems, Inc., Knoxville, TN). The resolution of the microPET scanner was $4.1mm^3$ [10]. The author participated in scanning and all subsequent stages of imaging.
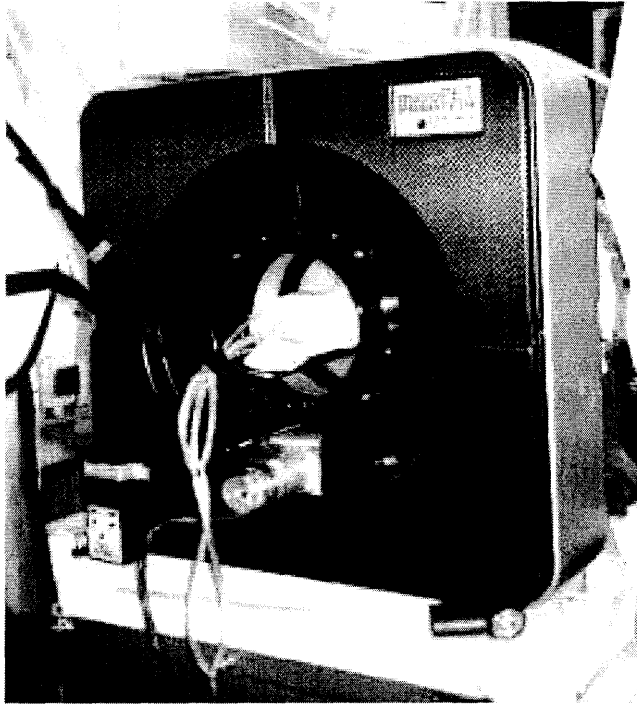
Figure 2-2. **microPET imaging set-up.** The mice subjects were positioned with their long axis parallel to the scanner [4].

2.4 Data Collection and Analysis Protocol

The microPET images were scanned and reconstructed using ASIPro© [11] by the author of this paper. After scanning for 50 minutes in continuous bed motion with FOV of 30 cm, data analysis was conducted with ASIPro VM. Regions of interest (ROIs) were drawn on averaged transverse images around the flank tumor, both right and left kidneys, liver, brain, leg muscle, and heart. The flank tumor was segregated into both a hot and "R" region – the former a categorization of the surface of the area which is vascularized, the latter representative of dead tissue within the grown tumor which lacks vascularization. ROIs for the heart ($0.067 \pm 0.007 \text{ cm}^2$) were drawn on the averaged first four frames of imaging. ROIs for all other organs ($0.13 \pm 0.016 \text{ cm}^2$) were drawn on the summation of all frames beyond those which represented the heart. Theses ROIs give the blood and tissue time-activity curves, respectively for all three mice analyzed for this

paper. A sample screen shot of ASIPro data collection and analysis is represented in *Figure 2-3*.
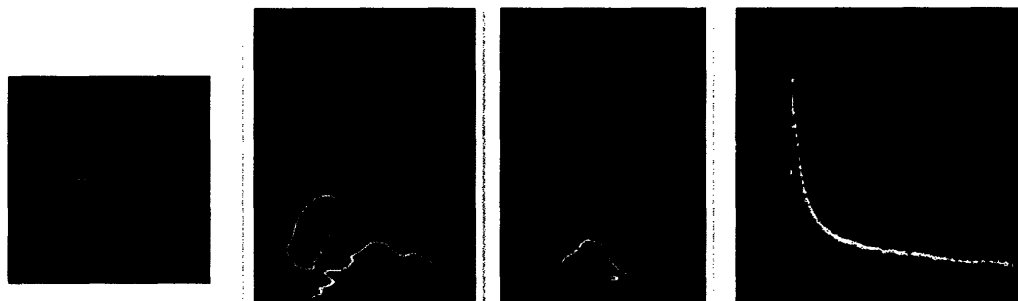
Figure 2-3. **Imaging murine cells using ASIPro data analysis techniques.** The first frame is a depth scan in the z-axis. The second frame is a prostate over-head scan, with regions of high radioactive activity in red. Green is an intermediate reflection of activity, while blue is the lowest level of qualitative activity. The final frame is the time-activity curve generated by the selected ROI.

2.5 Compartment Modeling Technique

Compartment models are the basis of most quantitative methodologies for physiologic analysis in nuclear medicine. Compartmental modeling is particularly applicable to PET scanning because tracer concentrations can be measured *in vivo* in absolute terms [12]. The model presented in this study will focus on blood flow through the prominent organs of the mouse: brain, two kidneys, liver, muscle, and grown tumor. The general mathematical framework used was COMKAT©, compatible with MATLAB© implementation.

Compartmental modeling is based on a building block approach for kinetic evaluation. In *Figure 2-4*, rectangular compartments represent vital portals of entrance and exit, while arrows represent blood flux. The syringe represents the point of injection. C_j denotes the concentration in compartment j; I_n denotes the concentration of input n. Compartment j is the recipient of fluxes from zero or more additional compartments i. Compartment j is the source of fluxes form zero or more additional compartments j.
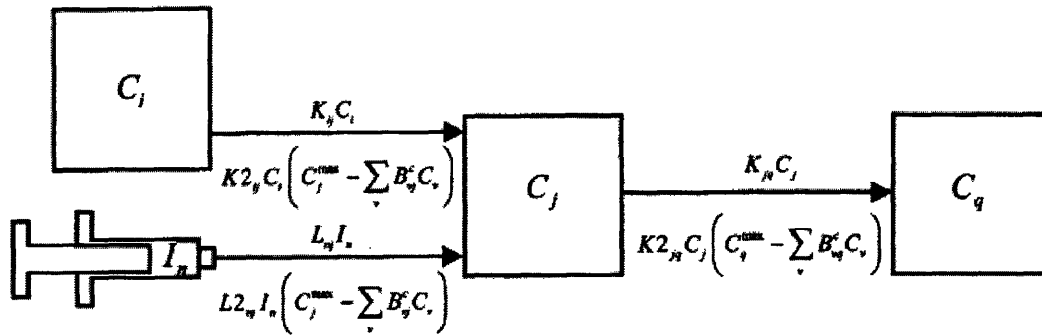
Figure 2-4. **COMKAT building-block modeling representation [12].**

A thorough application of COMKAT procedure and analysis was implemented to the extent of this study.

2.6 *Mathematical Modeling*

The 3-compartmental model used to describe the kinetics of $[^{18}F]FHBG$ accumulation is illustrated in *Figure 2-5*. k_1 (ml/min/ml), k_2 (min^{-1}), k_3 (min^{-1}), and k_4 (min^{-1}) are kinetic modeling constants. k_1 is derived to represent inward transport; k_2 is derived to represent outward transport; k_3 is derived to represent phosphorylation of $[^{18}F]FHBG$; k_4 is derived to represent dephosphorylation of the product and will be assumed negligible during this study as the results have been revealed as extremely small after calculation.

In *Figure 2-5*, the initial injection compartment will be modeled by the time activity curve of the heart, as it is the source of all blood flow. The organ compartment will be fed with the time activity of curve of the organ under study, while the last, output compartment will be parameter dependent upon the thymidine kinase phosphorylation reaction that occurred within the particular organ. In other words, the 3-compartmental model consists of $[^{18}F]FHBG$ in plasma, unmetabolized $[^{18}F]FHBG$ in tissue

(extravascular and intravascular), and metabolized [^{18}F]FHBG in tissue. The separation

between the second and third compartments represents the phosphorylation of
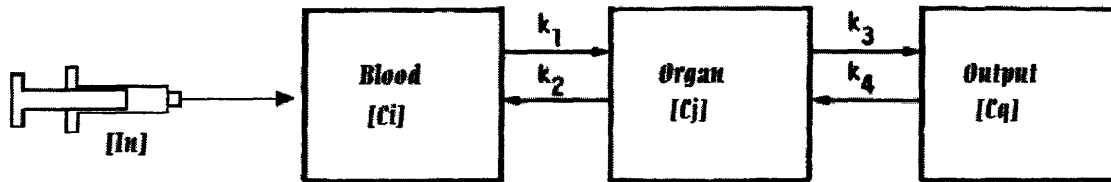
[^{18}F]FHBG.

Figure 2-5. 3-Compartment modeling of [^{18}F]FHBG phosphorylation. Included are COMKAT modeling designations as used in *Figure 2-4* for clarification.

This model is an extension of Sokoloff et al.'s three-compartmental model of

[^{14}C]deoxyglucose metabolism by phosphorylation enzyme hexokinase developed in

1977 [13]. Consistent with Sokoloff's model, the compartmental model used in this

study used similar assumptions:

1. [^{18}F]FHBG metabolism in tissues is in a steady state. The metabolic rate of [^{18}F]FHBG by TK and concentrations of all substrates and intermediates of the pathway are constant during time of study.

2. The phosphorylation of [^{18}F]FHBG by endogenous thymidine kinase (TK1 and TK2) is negligible.

3. Phosphorylated [^{18}F]FHBG cannot directly exit out of the cell.

4. Uptake of [^{18}F]FHBG is not flow limited.

5. Stereochemistry – that is the geometrical differences of the R and S forms of [^{18}F]FHBG – are ignored. R and S designation refers to the chirality of the molecule. We may assume that transport, metabolism, and clearance are equal for both R and S forms.

6. The transport of [^{18}F]FHBG has first-order kinetics between compartments. The system is linear.

7. k_4 is equal to zero, as dephosphorylation is negligible and not statistically relevant to the model.

The mathematical representation of the compartmental model is a system of ordinary linear differential equations. Its solution is the input, injection equation convolved with a sum of exponential expressions. An extensive mathematical treatment of the model is presented by Sokoloff.

2.6.1 Error Propagation in Mathematical Modeling

Noise in the PET data was assumed to be noise from body motion, organ motion, and reconstruction. The noise is Poisson distributed, and all other sources of noise were assumed to be negligible for counting statistics.

3. Results

3.1 ASIPro Collection of Time-Activity Curves by Organ

Figures 3-1 through 3-6 show averaged data collected from microPET scanning of mice in Groups A, B, and C. The tumor data, presented in *Figure 3-6,* was collected from mice in Group C only, and the Hot Tumor (the outside surface of the tumor receiving a vascular supply) was differentiated from the rest of the tumor (R-Tumor) which lacks a vascular supply.
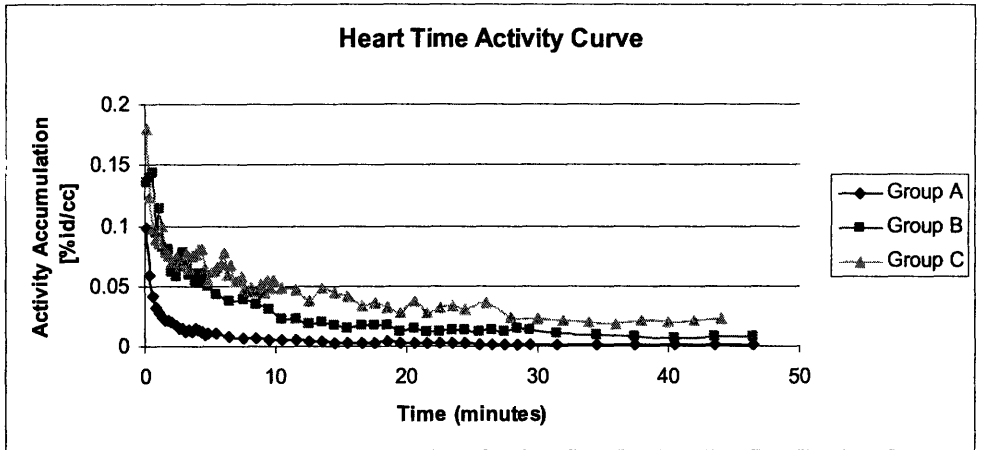
Figure 3-1. Heart Time-Activity Curve for mice in Groups A, B, and C
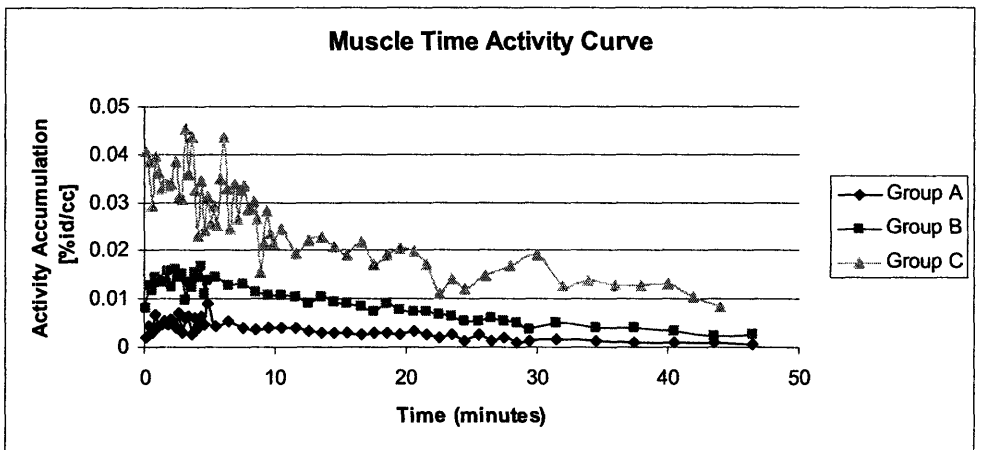
Figure 3-2. Muscle Time-Activity Curve for mice in Groups A, B, and C
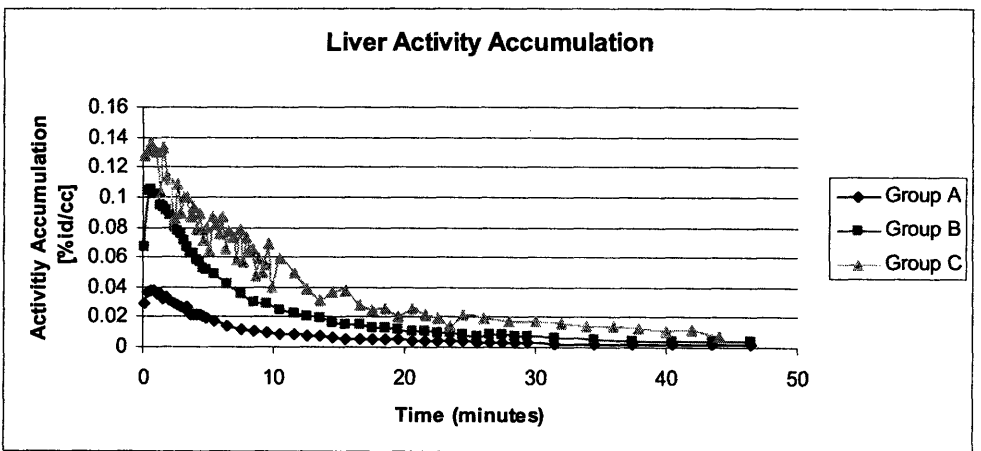
Figure 3-3. Liver Time Activity-Curve for mice in Groups A, B, and C
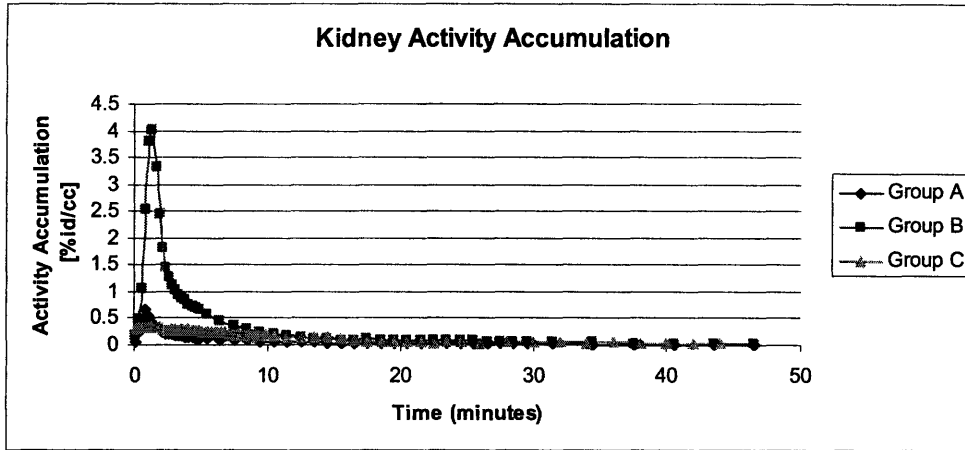
Figure 3-4. **Kidney Time-Activity Curve for mice in Groups A, B, and C**
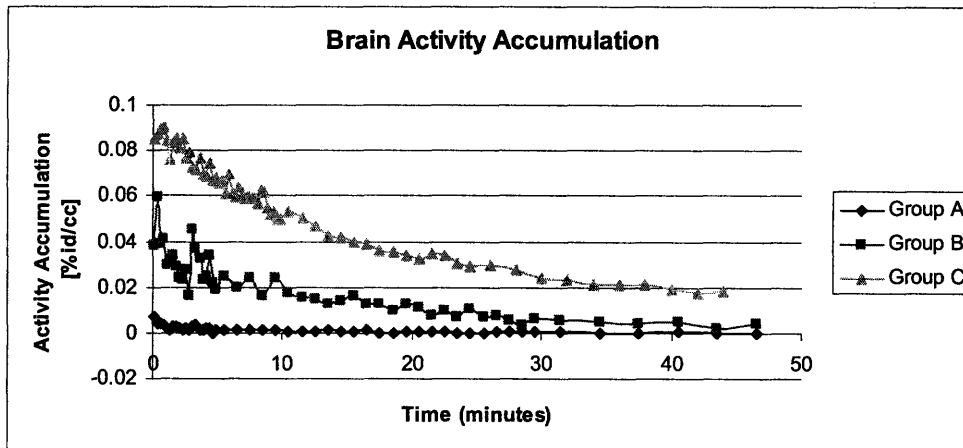
Figure 3-5. **Brain Time-Activity Curve for mice in Groups A, B, and C**
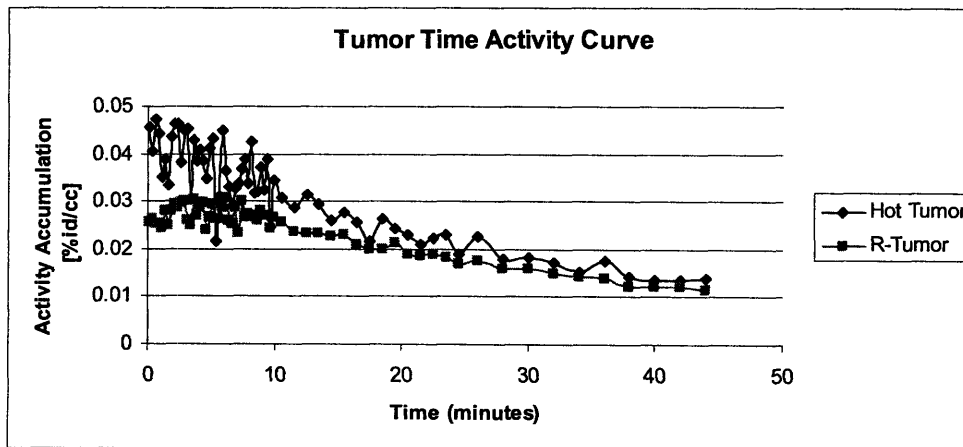
Figure 3-6. **Tumor Time-Activity Curve for mice in Group C**

3.2 Construction of COMKAT Modeling

Figure 2-5 represents a simplified model of compartmentalized flux entry and exit. The flux equals the unimolecular rate constant multiplied by the concentration of the source compartment or input and the concentration of the receiving compartment.

The model of *Figure 3-7* was used in this study and involves a single input of radioactive ligand [^{18}F]FHBG – a model with in and out flow kinetics.
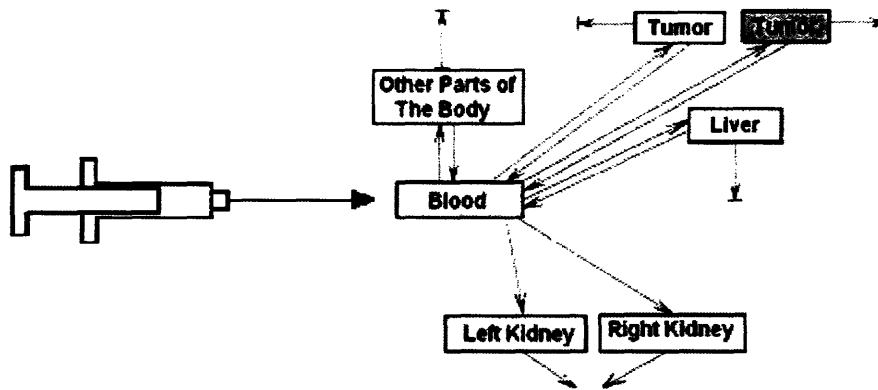
Figure 3-7. **Compartmental scheme for murine study.** The scheme provides an applicable compartmental model. The filled-in tumor compartment represents the "hot" region of the tumor. Other parts of the body were modeled by muscle tissue. The blood, or the input source, was measured by activity in the heart. The output from the kidneys exits the body, while the output for all other organs is strictly a reflection of phosphorylation process.

3.3 MATLAB Coding for 3-Comparmental Model

COMKAT was implemented using a code written in MATLAB programming scheme by the author. The coding is included in *Appendix 1*.

The resulting output (k_1, k_2, k_3) of the implementation of the code is included in *Tables 3-1, 3-2,* and *3-3*.

Table 1-1. k_1 modeling parameters for Groups A, B, and C

Organ	Group A – k1 (ml/min/ml)	Group B – k1 (ml/min/ml)	Group C – k1 (ml/min/ml)
Muscle	0.127	0.251	10.456
Kidney	10.209	34.517	6.695
Liver	1.528	3.048	3.110
Brain	0.101	2.859	9.407
Hot Tumor			21.096
R-Tumor			3.478

Table 3-2. k_2 modeling parameters for Groups A, B, and C

Organ	Group A – k2 (min^{-1})	Group B – k2 (min^{-1})	Group C – k2 (min^{-1})
Muscle	1.242	2.023	28.447
Kidney	0.857	2.890	1.762
Liver	2.066	4.286	2.448
Brain	1.466	8.682	11.998
Hot Tumor			47.060
R-Tumor			12.945

Table 3-3. k_3 modeling parameters for Groups A, B, and C

Organ	Group A – k3 (min^{-1})	Group B – k3 (min^{-1})	Group C – k3 (min^{-1})
Muscle	0.128	0.249	0.170
Kidney	4.00E-02	10.417	1.00E-03
Liver	0.273	0.948	7.49E-01
Brain	0.213	0.765	0.554
Hot Tumor			0.816
R-Tumor			0.155

Graphical representations, with error consideration, are provided in *Figures 3-8*, *3-9*, and *3-10*.
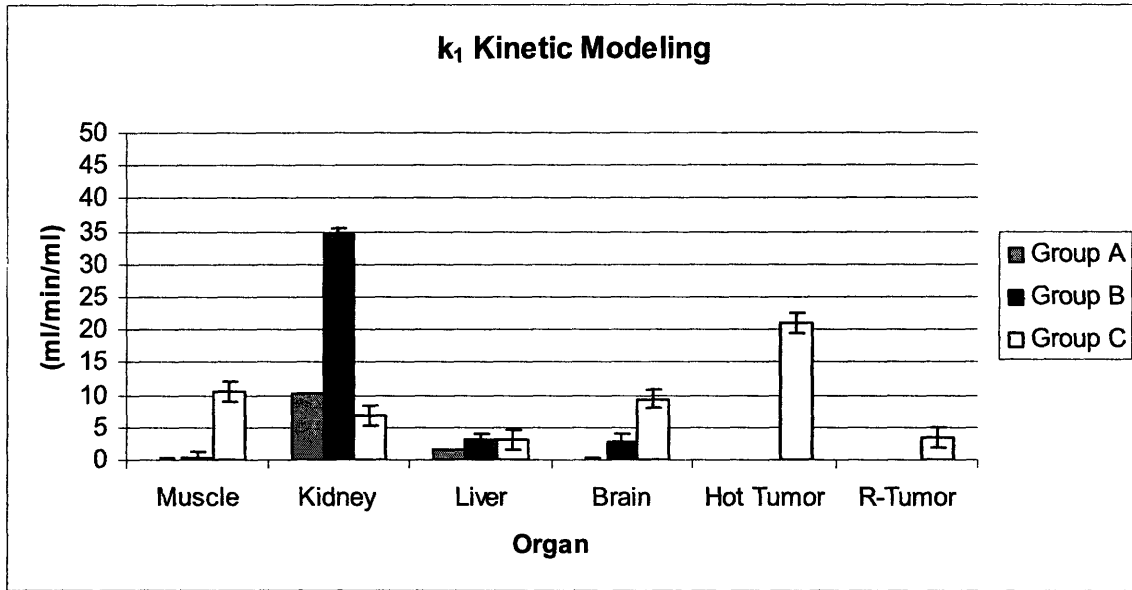
Figure 3-8. **Graphical representation of** k_1 **modeling by organ distribution in Group A, B, and C, with standard deviation error approximation**
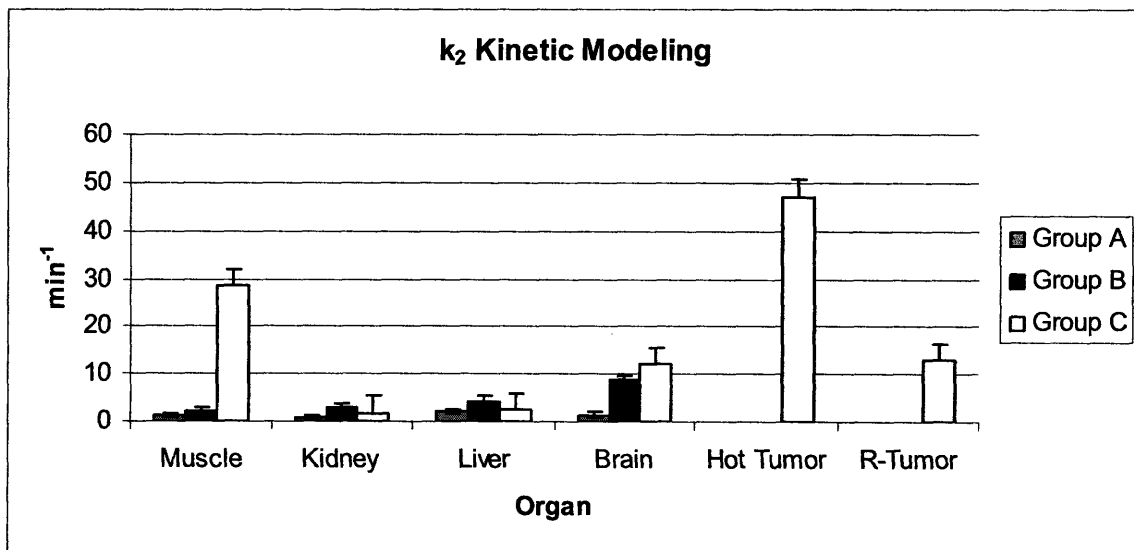
Figure 3-9. **Graphical representation of** k_2 **modeling by organ distribution in Group A, B, and C, with standard deviation error approximation**
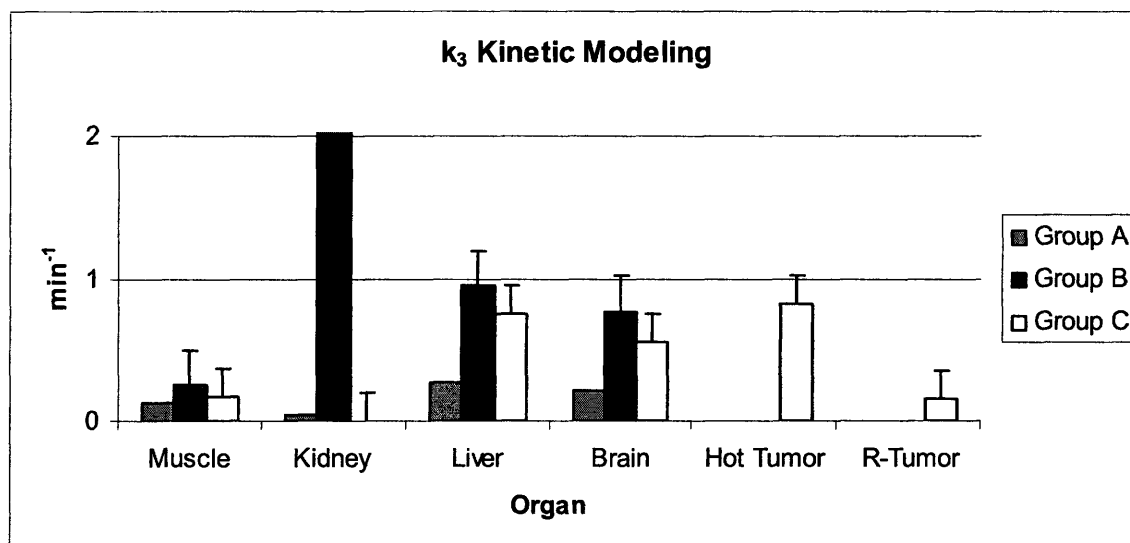
Figure 3-10. Graphical representation of k_3 modeling by organ distribution in Group A, B, and C, with standard deviation error approximation

3.4 MATLAB Coding for Complete Mouse Fitting

Once k_1, k_2, and k_3 parameters were calculated, a full-system fitting of mice in Group A, B, and C were coded using more intricate COMKAT implementation in MATLAB. The code, written by the author, is included in *Appendix 2*.

4. Discussion and Analysis

4.1 Time-Activity Curve Interpretation

A qualitative analysis of the activity biodistribution of intravenously injected [^{18}F]FHBG shows the heart, liver, and kidney decreased to baseline levels of activity in all three experimental groups of mice during the 50 minute scanning period. The time-activity curve of the brain in Group A decreased to baseline levels of activity after a transient level of activity. The time-activity curve of the brain approached baseline levels of activity in Groups A and B. Group C, however, did not approach baseline levels. It

may be inferred that the 50 minute scanning period was not long enough for the blood-brain barrier to be cleared by the radioactive compound. The blood-brain barrier presents a biological mechanism that is not easily modeled by the kinetic parameters calculated in this study.

[^{18}F]FHBG has very low penetration through the blood-brain barrier which is shown in the brain of Group A. However, injection of the virus enhances general blood flow and correspondingly values exhibited by Group B and C are significantly higher than those exhibited by Group A.

The kidney activity curves were unique in the presence of initial peaks, particularly prominent in Group B testing. The intensity of the signal of Group B particularly remained high in comparison with all other organs. The kidney is largely responsible for outflow, or metabolic excretion, of the product and therefore peaks in metabolic activity may be expected.

On the basis of the patterns of biodistribution, it may be deduced that imaging of the HSV1-tk gene with [^{18}F]FHBG is efficient, and successful, in most anatomical regions except the lower abdomen due to high bladder activity and the central nervous system due to restricted passage of [^{18}F]FHBG across the blood-brain barrier.

It may be clinically prudent to wait a controlled length of time (on the order of 20 minutes) after injection of radioactive tracer before HSV1-tk signals can be recorded. In the liver and kidneys the signals may initially be too high, while the muscle activity curve requires a period of approximately 10 minutes to stabilize statistically significant perturbations. It is possible that muscle tissue is most susceptible to background signal noise.

In a clinically setting, it would be advisable for patients to urinate before injecting with the radioactive dose.

4.2 Parameters of 3-Compartmental Model Interpretation

k_1 and k_2 are the parameters related to transport of the probe. To take an organ by organ approach, the muscle tissue's k_1 parameter is virtually negligible in both Group A and Group B mice. The inflow of probe to the muscle tissue, under conditions in which the virus is either absent or present, is comparable to the Group A parameter in the brain. As was noted previously, Group A does not exhibit any penetration of the blood-brain barrier.

The blood-brain barrier is blocked to [^{18}F]FHBG when the virus is not present. When the virus contributes to the system, however, uptake of [^{18}F]FHBG is enhanced. Tumor activity seems to enhance uptake of [^{18}F]FHBG further in the brain.

The liver's k_1 parameter remains comparable in all experimental groups within standard deviation. As expected, the hot tumor region receives a high level of blood flow. It is greater than the blood flow to the R-tumor, and an overall leader in comparison with all other organs. The kidney's k_1 parameter is dubious, as it is inherently dependent upon the collection of urine.

k_3 parameterizes enzymatic phosphorylation by TK. The data modeling presented metabolic phosphorylation to be within comparable limits in the muscle between all three groups. Mean standard deviation did not allow for a significant differentiation of muscle tissue phosphorylation in the three groups. Phosphorylation in the muscle takes place at a similar level to that of the brain of Group A, as well as the R-tumor. The R-tumor receives no virus, and therefore it is expected that it behaves similar to muscle tissue.

k_3 of the hot tumor was comparable to the k_3 of the liver when the virus was present. It is thus notable to equate phosphorylation in cancer tissue under viral oncolytic treatment conditions with the environment of the liver under viral treatment.

The virus enhances blood flow to the brain in a biological mechanism that allows it to cross the blood-brain barrier. Phosphorylation is prominently enhanced in the hot tumor as compared to in the R-tumor.

4.3 Additional Applications of Kinetic Parameters

Using the individual three kinetic parameters calculated in this study. The ratio k_1/k_2 (ml/ml) corresponds to the distribution volume of free or nonphosphorylated [^{18}F]FHBG. The phosphorylation fraction (PF) of [^{18}F]FHBG can be represented by the ratio $k_3/(k_2 + k_3)$. It can be interpreted as a reflection of the disposition for nonphosphorylated [^{18}F]FHBG within the organ to be phosphorylated.

5. Conclusions

Viral oncolysis has presented promising results in reduction of tumor size and preferential infection of tumor cells rather than healthy cells in preclinical models [14]. An assessment of sites, magnitude, and kinetic behavior of viral replication is necessary to correlate vector design and dose schedule with specificity of efficiency, specificity, and toxicity. Although radiolabel accumulation is seen to peak by 6 hours after injection [10], this study monitored the first 50 minutes after injection. The time frame secured risk against toxicity consideration, as well as attempting to collect data that is not skewed by cell lysis that may result from viral replication.

The time-activity curves generated for the vital organs of Groups A, B, and C underscored several key conclusions. The heart does not undergo significant [^{18}F]FHBG accumulation, as it delivers blood flow through the mouse. Muscle [^{18}F]FHBG accumulation is erratic until a stabilization is reached. Group C muscle accumulation was significantly more extensive than evident in both Group A and B. Liver [^{18}F]FHBG accumulation can be likened to the behavior of the heart in all groups. Kidney [^{18}F]FHBG accumulation is unreliable as it is heavily dependent upon urine excretion.

The kinetic modeling developed in this study monitored viral oncolysis by implementing a 3-Compartmental Model with distinct parameters. The conclusions derived from the time-activity curves were again largely re-emphasized by k_1, k_2, and k_3 calculation, with specific attention paid to the behavior of the brain and tumor. Value comparison for the brain suggests that phosphorylation and viral transport occur under a unique mechanism that is less predictable than most other mammalian organs. The blood-brain barrier offers an obstacle for blood-flow that is met by the virus well. The virus enhances blood flow.

The hot tumor is active in all parameters of kinetic modeling, with a k_2 that exceeds its k_1, and therefore a significant source of blood out-flow. k_3 of the hot tumor indicates that the tumor is active in phosphorylation, while the R-tumor is as inactive as muscle tissue.

The COMKAT-inspired MATLAB code in *Appendix 1* produced precise results for parameter modeling, with error comfortably seated within reasonable bounds. The full-system modeling developed by the MATLAB code in *Appendix 2* fits all parameters into a complete biological system, coupling all 3-Compartmental Models. It is a

successful check for accuracy and reliability of results. When implemented, all parameters were within standard deviation.

5.1 Direction of Future Studies

This study set a framework for controlling dose and distribution under viral oncolytic treatment. Before treatment can be taken from the murine to the human, maximum tolerated dose must be established at a variety of pfu. Additional studies must be performed to compare behavior, specifically of the tumor and brain, under varying pfu measurements beyond the 10^7 pfu that this study focused upon. Explorative work may be done in regimens consisting of multiple doses of virus over an extended length of time. Similar studies may be formulated to assess host immune response elicited against both the virus and the tumor.

A new phase of studies may be undertaken by recovering virus from treated tumors in order to demonstrate the rate and efficiency of viral replication. Such results are relevant when assessing the efficacy of viral oncloytic therapy.

The most conspicuous questions raised in this study concerned the characterization of the blood-brain barrier under viral oncolytic treatment. Vectors must be developed that will target the brain more successfully.

As is usually the case with oncolytic studies, adjunctive therapy must be considered – namely ionizing radiation to shrink the tumor.

The 3-Compartmental Model must be expanded to include other vital organs: the stomach, spleen, etc.

References

[1] J. T. Mullen, K. K. Tanabe. New Approaches to the Treatment of Hepatic

Malignancies: Viral Oncolysis for Malignant Liver Tumors. *Annals of Surg Oncology*,

10(6): 596-605, 2003.

[2] J. Sinkovics, J. Horvath. New developments in the virus therapy of cancer: a

historical review. *Intervirology* 36(4): 192-214, 1993.

[3] S. R. Cherry, Y. Shao, R. W. Silverman, A. Chatziioannou, K. Meadors, S. Siegel, A.

Boutefnouchet, A. T. Farquhar, J. Young, W. F. Jones, D. Newport, C. Moyers, M.

Andreaco, M. Paulus, D. Binkley, R. Nutt, M. E. Phelps. MicroPET: A high resolution

PET scanner for imaging small animals. *IEEE Transactions on Nuc. Science*, 44: 1161-

1166, 1997.

[4] D. Kuruppu. "Imaging Viral Oncolysis by MicroPET." Harvard Medical School.

Massachusetts General Hospital, Boston. 04 Nov. 2005. Powerpoint Presentation.

[5] R. L. Martuza. Conditionally replicating herpes vectors for cancer therapy. *J

Clinical Investigation*, 105(7): 841-846, April 2000.

[6] J. J. Bennett, J. Tjuvajev, P. Johnson, M. Doubrovin, t. Akhurst, S. Malhorltra, T.

Hackman, J. Balatoni, R. Finn, S. Larson, H. Federoff, R. Blasberg, Y. Fong. Positron

emission tomography imaging for herpes virus infection: Implications for oncolytic viral treatments of cancer. *Nature Medicine*, 7(7): 859-863, July 2001.

[7] W. B. Mahoney, B. A. Domin, R. T. McConnell, T.P. Zimmerman. Acyclovir Transport into Human Erthrocytes. *J Biol Chem*, 263(19): 9285-9291, July 1988.

[8] W. B. Mahoney, B. A. Domin, R. T. McConnell, T. P. Zimmerman. Ganiclovir permeation of the human erythrocyte membrane. *Biochem Pharmacol*. 41(2): 263-71, July 1988.

[9] J. G. Tjuvajev, G. Stockhammer, R. Desair, H. Uehara, H. Watanabe, B. Gansbacher, R. G. Blasberg. Imaging the expression of transfected genes *in vivo*. *Cancer Res*, 55(24): 6126-6132, 1995.

[10] D. Kuruppu, A.L. Brownell, A. Zhu, M. Yu, X. Wang, Y. Kulu, B. Fuchs, H. Kawasaki, K. Tanabe. Positron Emission Tomography of Herpes Simplex Virus 1 Oncolysis. *Cancer Res*, 67(7): 3295-3300, April 2007.

[11] *ASIPro: Acquisition Sinogram and Image Processing*. Malvern, PA: Siemens Medical, 2005.

[12] R. F. Muzic, Jr., S. Cornelius. COMKAT: Compartment Model Kinetic Analysis Tool. *J Nuclear Medicine*, 42(4): 636-645, April 2001.

[13] L. Sokoloff, M. Reivich, C. Kennedy, M. H. Des Rosiers, C. S. Patlak, K. D. Pettigrew, O. Sakurada, M. Shinohara. The [^{14}C]deoxyglucose method for the measurement of local cerebral glucose utilization: theory, procedure, and normal values in the conscious and anesthetized albino rat. *J. Neurochemistry*, 28: 897-916, 1977.

[14] R. Rampling, G. Cruickshank, V. Papanastassiou, J. Nicoll, D. Hadley, D. Brenna, R. Petty, A. MacLean, J. Harland, E. McKie, R. Mabbs, M. Brown. Toxicity evaluation of replication-competent herpes simplex virus (ICP 34.5 null mutant 1716) in patients with recurrent malignant glioma. *Gene Ther*, 7(10): 859-66, May 2000.

Appendix 1

```
% create new, empty model
% current version: $Revision: 1.1 $ $Date: 2006/02/01 20:16:57 $
bfcm = compartmentModel;


% add compartments
bfcm = addCompartment(bfcm, 'C1');
bfcm = addCompartment(bfcm, 'C2');
bfcm = addCompartment(bfcm, 'J');


% define and add input
inputboxdata = load('inputboxdata.txt')'; % input heart data points
here
compartmentdata = load('compartmentdata.txt')'; % compartment data
(e.g. liver, muscle, etc.) points here
starttimes = load('starttimes.txt')'; % input time points here
stoptimes = load('stoptimes.txt')'; % input time points here


sa0 = 1; % specific activity at t=0
dk = iso2lambda('F-18', 'seconds'); % F-18 decay constant.


bfcm = addInput(bfcm, 'Im', sa0, dk, 'ppval', interp1(starttimes,
inputboxdata, 'linear', 'pp'));


bfcm = set(bfcm, 'Optimizer', 'lmwls');    % optimizer


% connect compartments and inputs
bfcm = addLink(bfcm, 'L', 'Im', 'C1', 'K1');
bfcm = addLink(bfcm, 'K', 'C1', 'J', 'K2');
bfcm = addLink(bfcm, 'K', 'C1', 'C2', 'K3');
bfcm = addLink(bfcm, 'K', 'C2', 'C1', 'K4');


% define values for K1, K2 ...
bfcm = addParameter(bfcm, 'K1', .5);
bfcm = addParameter(bfcm, 'K2', .5);
bfcm = addParameter(bfcm, 'K3', .5);
bfcm = addParameter(bfcm, 'K4', .5);


% specify output
Wlist = {...  % compartment contrib.
    'C1', '1',
    'C2', '1';
};
Xlist = {... % input contrib.
};
bfcm = addOutput(bfcm, 'PET', Wlist, Xlist);


bfcm = set(bfcm, 'ScanTime', [starttimes' stoptimes']);
[PET, PETIndex] = solve(bfcm);
figure(1) % Dry run of model for output compartment data
plot(0.5*sum(PET(:,[1 2]),2),PET(:,3),'.')
```

```
% for fitting part of example, use model to generate sample output
bfcm=set(bfcm,'ParameterValue','K1',0.4);
bfcm=set(bfcm,'ParameterValue','K2',0.95);
bfcm=set(bfcm,'ParameterValue','K3',0.95);
bfcm=set(bfcm,'ParameterValue','K4',0.95);
[PET, PETIndex] = solve(bfcm);

%ed=PET(:,3);
ed = compartmentdata';
bfcm=set(bfcm,'ExperimentalData', ed);

% define initial guess and lower and upper bounds
bfcm=addSensitivity(bfcm, 'K1', 'K2', 'K3', 'K4');
pinit = [1.0 1.0 1.0 1.0];
lb = [.001 .001 .001 .001];
ub = [100 100 100 100];

% solve for model output at initial guess
bfcm=set(bfcm,'ParameterValue','K1',pinit(1));
bfcm=set(bfcm,'ParameterValue','K2',pinit(2));
bfcm=set(bfcm,'ParameterValue','K3',pinit(3));
bfcm=set(bfcm,'ParameterValue','K4',pinit(4));
[PET, PETIndex] = solve(bfcm);

% plot experimental data (dots) along with inital guess
figure(2) % Dry run of model vs. actual output compartment data
plot(0.5*sum(PET(:,[1 2]),2),ed,'.')
hold on
stairs2(PET(:,[1 2]),PET(:,3))
hold off

% fit experimental data
[pest,modelfit] = fit(bfcm, pinit, lb, ub);
figure(3) % Fit model vs. actual output compartment data
plot(0.5*sum(PET(:,[1 2]),2),ed,'.')
hold on
stairs2(PET(:,[1 2]),modelfit)
hold off

pest % Model's estimated parameters

err = modelfit - ed;
outputsize = size(err);
rmserr = sqrt(sum(err .* err)/outputsize(1)) % RMS error

k1fit = pest(1)
k2fit = pest(2)
k3fit = pest(3)
k4fit = pest(4)
```

Appendix 2

I. Step Function Defined

```
function y = steppy(p, t)
%p(1) is the time at which the step ends, (2) is the height of the step
%t is the times to calculate at

m=0;
[m,n] = size(t);
y=zeros(m,n);
for i=1:m
    for j=1:n
        if t(i,j) <= p(1)
            y(i,j) = p(2);
        else
            y(i,j) = 0;
        end
    end
end
```

II. Complete Code

```
% create new, empty model
% current version: $Revision: 1.1 $ $Date: 2006/02/01 20:16:57 $
bfcm = compartmentModel;

% add compartments
bfcm = addCompartment(bfcm, 'Cheart');
bfcm = addCompartment(bfcm, 'Cmuscle');
bfcm = addCompartment(bfcm, 'Chottumor');
bfcm = addCompartment(bfcm, 'Ckidney');
bfcm = addCompartment(bfcm, 'Cliver');
bfcm = addCompartment(bfcm, 'Cbrain');
bfcm = addCompartment(bfcm, 'Cjunk');

% define and add input
heartdata = load('heartdata.txt')';
muscledata = load('muscledata.txt')';
hottumordata = load('hottumordata.txt')';
kidneydata = load('kidneydata.txt')';
liverdata = load('liverdata.txt')';
braindata = load('braindata.txt')';
starttimes = load('starttimes.txt')'; % input time points here
stoptimes = load('stoptimes.txt')'; % input time points here

sa0 = 1; % specific activity at t=0
dk = iso2lambda('F-18', 'seconds'); % F-18 decay constant.

bfcm = addInput(bfcm, 'Iinj', sa0, dk, 'steppy', [.5, 1.0]);

bfcm = set(bfcm, 'Optimizer', 'lmwls');    % optimizer
```

```
% connect compartments and inputs
bfcm = addLink(bfcm, 'L', 'Iinj', 'Cheart', 'Kinj');
bfcm = addLink(bfcm, 'K', 'Cheart', 'Cmuscle', 'Khm');
bfcm = addLink(bfcm, 'K', 'Cmuscle', 'Cheart', 'Kmh');
bfcm = addLink(bfcm, 'K', 'Cheart', 'Chottumor', 'Kht');
bfcm = addLink(bfcm, 'K', 'Chottumor', 'Cheart', 'Kth');
bfcm = addLink(bfcm, 'K', 'Cheart', 'Ckidney', 'Khk');
bfcm = addLink(bfcm, 'K', 'Ckidney', 'Cheart', 'Kkh');
bfcm = addLink(bfcm, 'K', 'Cheart', 'Cliver', 'Khl');
bfcm = addLink(bfcm, 'K', 'Cliver', 'Cheart', 'Klh');
bfcm = addLink(bfcm, 'K', 'Cheart', 'Cbrain', 'Khb');
bfcm = addLink(bfcm, 'K', 'Cbrain', 'Cheart', 'Kbh');
bfcm = addLink(bfcm, 'K', 'Ckidney', 'Cjunk', 'Kkj');

% define values for K1, K2 ...
bfcm = addParameter(bfcm, 'Kinj', 1.0);
bfcm = addParameter(bfcm, 'Khm', .5);
bfcm = addParameter(bfcm, 'Kmh', .5);
bfcm = addParameter(bfcm, 'Kht', .5);
bfcm = addParameter(bfcm, 'Kth', .5);
bfcm = addParameter(bfcm, 'Khk', .5);
bfcm = addParameter(bfcm, 'Kkh', .5);
bfcm = addParameter(bfcm, 'Khl', .5);
bfcm = addParameter(bfcm, 'Klh', .5);
bfcm = addParameter(bfcm, 'Khb', .5);
bfcm = addParameter(bfcm, 'Kbh', .5);
bfcm = addParameter(bfcm, 'Kkj', .5);

% specify output
bfcm = addOutput(bfcm, 'PETheart', {'Cheart', '1'}, {});
bfcm = addOutput(bfcm, 'PETmuscle', {'Cmuscle', '1'}, {});
bfcm = addOutput(bfcm, 'PETtumor', {'Chottumor', '1'}, {});
bfcm = addOutput(bfcm, 'PETkidney', {'Ckidney', '1'}, {});
bfcm = addOutput(bfcm, 'PETliver', {'Cliver', '1'}, {});
bfcm = addOutput(bfcm, 'PETbrain', {'Cbrain', '1'}, {});

bfcm = set(bfcm, 'ScanTime', [starttimes' stoptimes']);
[PET, PETIndex] = solve(bfcm);
figure(1) % Dry run of model for output compartment data
plot(0.5*sum(PET(:,[1 2]),2),PET(:,3),'.')

% for fitting part of example, use model to generate sample output
bfcm=set(bfcm,'ParameterValue','Kinj',1.0);
bfcm=set(bfcm,'ParameterValue','Khm',0.95);
bfcm=set(bfcm,'ParameterValue','Kmh',0.95);
bfcm=set(bfcm,'ParameterValue','Kht',0.95);
bfcm=set(bfcm,'ParameterValue','Kth',0.95);
bfcm=set(bfcm,'ParameterValue','Khk',0.95);
bfcm=set(bfcm,'ParameterValue','Kkh',0.95);
bfcm=set(bfcm,'ParameterValue','Khl',0.95);
bfcm=set(bfcm,'ParameterValue','Klh',0.95);
bfcm=set(bfcm,'ParameterValue','Khb',0.95);
bfcm=set(bfcm,'ParameterValue','Kbh',0.95);
bfcm=set(bfcm,'ParameterValue','Kkj',0.95);
[PET, PETIndex] = solve(bfcm);
```

```
ed = [heartdata' muscledata' hottumordata' kidneydata' liverdata'
braindata'];
bfcm=set(bfcm,'ExperimentalData', ed);

% define initial guess and lower and upper bounds
bfcm=addSensitivity(bfcm, 'Kinj', 'Khm', 'Kmh', 'Kht', 'Kth', 'Khk',
'Kkh', 'Khl', 'Klh', 'Khb', 'Kbh', 'Kkj');
pinit = [1.0 1.0 1.0 1.0 1.0 1.0 1.0 1.0 1.0 1.0 1.0 1.0];
lb = [.001 .001 .001 .001 .001 .001 .001 .001 .001 .001 .001 .001];
ub = [100 100 100 100 100 100 100 100 100 100 100 100];

% solve for model output at initial guess
bfcm=set(bfcm,'ParameterValue','Kinj',pinit(1));
bfcm=set(bfcm,'ParameterValue','Khm',pinit(2));
bfcm=set(bfcm,'ParameterValue','Kmh',pinit(3));
bfcm=set(bfcm,'ParameterValue','Kht',pinit(4));
bfcm=set(bfcm,'ParameterValue','Kth',pinit(5));
bfcm=set(bfcm,'ParameterValue','Khk',pinit(6));
bfcm=set(bfcm,'ParameterValue','Kkh',pinit(7));
bfcm=set(bfcm,'ParameterValue','Khl',pinit(8));
bfcm=set(bfcm,'ParameterValue','Klh',pinit(9));
bfcm=set(bfcm,'ParameterValue','Khb',pinit(10));
bfcm=set(bfcm,'ParameterValue','Kbh',pinit(11));
bfcm=set(bfcm,'ParameterValue','Kkj',pinit(11));
[PET, PETIndex] = solve(bfcm);


% plot experimental data (dots) along with inital guess
figure(2) % Dry run of model vs. actual output compartment data
plot(0.5*sum(PET(:,[1 2]),2),ed,'.')
hold on
stairs2(PET(:,[1 2]),PET(:,3))
hold off

% fit experimental data
[pest,modelfit] = fit(bfcm, pinit, lb, ub);
figure(3) % Fit model vs. actual output compartment data
plot(0.5*sum(PET(:,[1 2]),2),ed,'.')
hold on
stairs2(PET(:,[1 2]),modelfit)
hold off

pest % Model's estimated parameters

err = modelfit - ed;
outputsize = size(err);
rmserr = sqrt(sum(err .* err)/outputsize(1)) % RMS error

kinjfit = pest(1)
khmfit = pest(2)
kmhfit = pest(3)
khtfit = pest(4)
Kthfit = pest(5)
khkfit = pest(6)
```

```
kkhfit = pest(7)
khlfit = pest(8)
klhfit = pest(9)
khbfit = pest(10)
kbhfit = pest(11)
kkjfit = pest(12)
```